

# Nanoscale

Accepted Manuscript



This is an *Accepted Manuscript*, which has been through the Royal Society of Chemistry peer review process and has been accepted for publication.

*Accepted Manuscripts* are published online shortly after acceptance, before technical editing, formatting and proof reading. Using this free service, authors can make their results available to the community, in citable form, before we publish the edited article. We will replace this *Accepted Manuscript* with the edited and formatted *Advance Article* as soon as it is available.

You can find more information about *Accepted Manuscripts* in the [Information for Authors](#).

Please note that technical editing may introduce minor changes to the text and/or graphics, which may alter content. The journal's standard [Terms & Conditions](#) and the [Ethical guidelines](#) still apply. In no event shall the Royal Society of Chemistry be held responsible for any errors or omissions in this *Accepted Manuscript* or any consequences arising from the use of any information it contains.

# Centimeter-scale-homogeneous SERS substrates with seven-order global enhancement through thermally controlled plasmonic nanostructures

Hongmei Liu,<sup>a</sup> Xinping Zhang,<sup>\*a</sup> Tianrui Zhai,<sup>a</sup> Thomas Sander,<sup>b</sup> Limei Chen,<sup>b</sup> and Peter J Klar<sup>b</sup>

<sup>a</sup> *Institute of Information Photonics Technology and College of Applied Sciences, Beijing University of Technology, Beijing 100124, P. R. China*

<sup>b</sup> *Institute of Experimental Physics I, Justus-Liebig-University, Heinrich-Buff-Ring 16, 35392 Giessen, Germany*

*\*Email: zhangxinping@bjut.edu.cn*

## ABSTRACT

Highly homogeneous surface-enhanced Raman scattering (SERS) substrates were produced in centimeter-scale by annealing solution processed gold nanoparticles into plasmonic nanoislands. The average size and separation of the nanoislands are controlled by tuning the annealing temperature. SERS measurements yield a global enhancement factor as large as  $10^7$  over an area of  $2 \times 2 \text{ cm}^2$  for samples annealed at temperatures ranging from 150 to 200°C. Spectral “mapping” of the SERS signal shows a homogeneous distribution of the hotspots with high contrast over the whole substrate. The relative standard deviation of the SERS signal is less than 5.4% over an area of  $50 \times 50 \text{ }\mu\text{m}^2$ . Theoretical simulations show strong dependence of the near-field electromagnetic enhancement on the size and the separation gap of the gold nanoislands. Both, average gap size and average nanoisland size increase with increasing annealing temperature. Intensive plasmonic coupling between the adjacent gold nanoislands leads to broadband resonance for samples annealed at 150 and 200 °C, so that laser excitation within the spectrum of plasmon resonance at 633 or 785 nm produced significantly enhanced SERS for 4-Mercaptopyridine molecules modified on the gold nanoislands.

**KEYWORDS:** Surface-enhanced Raman spectroscopy, hotspot, Raman mapping, solution processed gold nanoislands

## 1 Introduction

Surface-enhanced Raman scattering (SERS) has attracted much interest since 1970s owing to its potential applications in ultrasensitive analysis<sup>1</sup>. The distinct advantage of SERS lies in the huge enhancement of the Raman signal, which serves as a fingerprint of molecular substances, enabling, in principle, detection and identification of analytes down to the single-molecule level. Therefore, SERS-based sensors may be used for detecting environmental pollutants, forbidden additives in food products, or residues of explosives, etc. and thus may contribute to solving major social problems such as preservation of the environment, guaranteeing food safety, or fighting terrorism. With the development of portable Raman spectroscopic devices, SERS-based onsite food safety detection<sup>2</sup> and environmental monitoring<sup>3</sup> are expected to become reality soon. However, reliable fabrication of large area SERS substrates at low costs is still a challenge because of difficulties in achieving reproducibly “hotspots” with high enhancement, high density, and homogeneous distribution over the entire area of the SERS substrate. The “hotspots” are generally defined as the locations of intensive plasmonic fields occurring in the gaps narrower than 10 nm between adjacent metallic nanostructures. SERS enhancement factor as high as  $\sim 10^{14}$  have been reported for individual hot spots. However, the average global enhancement on a SERS substrate is more crucial for practical applications. It depends not only on the local enhancement of the individual hot spots, but also on their density and homogeneity in distribution. In order to obtain such hotspot arrangements, various methods such as electron beam lithography,<sup>4</sup> nanosphere lithography,<sup>5</sup> focused ion-beam patterning,<sup>6</sup> self-assembly,<sup>7</sup> and other strategies,<sup>8-10</sup> have been employed. However, there are limitations on controllability and reproducibility for obtaining high-quality SERS substrates. Capillary-assisted

assembly is reported as an economic technique for producing SERS substrates reproducibly, however, but large-scale homogeneity is still a big challenge for this method.<sup>8</sup> Copolymer-template self-assembling provides a simple method for preparing the SERS substrates with a high degree of controllability.<sup>7</sup> However, the copolymer template is difficult to remove by lift-off process and the residues lead to poor signal to noise ratio in practical applications.

In this work, we report an approach based on solution processing of colloidal gold nanoparticles to prepare hotspot-active SERS substrates with a large-area homogeneity in a highly reproducible way. Spin-coating of the gold nanoparticles in colloids combined with a subsequent annealing process has proven to be a simple and reliable fabrication process. It enables a correlated control of the size and separation distance (or gap width) of gold nanoislands produced on the transparent glass substrates. Optimized global SERS enhancement factors as large as  $10^7$  have been achieved over a whole substrate area of  $2 \times 2 \text{ cm}^2$  for samples annealed in the temperature range from 150 to 200 °C. Furthermore, this enhancement factor was found to vary with a relative standard deviation as small as 5.4% as measured over an area of  $50 \times 50 \text{ }\mu\text{m}^2$ . Therefore, this kind of solution-processed SERS substrates is a potential candidate for commercialized devices combining the advantages of huge signal enhancement, high quality, large-area homogeneity, and low costs.

## **2 Solution-processed SERS substrates with controllable size/gap configuration of the gold nanoisland structures**

The 1-hexanethiol modified gold nanoparticles with a mean diameter smaller than 5 nm were synthesized as previously reported.<sup>11</sup> 1-hexanethiol modified gold nanoparticles have been used as the precursor in order to improve the stability of the final product. Colloidal solution of the gold nanoparticles was prepared by dissolving

the powder of ligand-covered gold nanoparticles into xylene with a concentration of 100 mg/ml, which was then spin-coated onto glass or silicon substrates to produce thin films of colloidal gold nanoparticles with sizes of 5 nm. In a subsequent annealing step performed in a furnace for 20 minutes, the gold nanoparticles are melted to form gold nanoislands. Controlling the annealing temperature, different sizes and different separation distances of the gold nanoislands may be produced on the substrate. Theoretical and experimental investigations have both shown that the melting point of the gold nanoparticle decreases sharply when its diameter is reduced to smaller than 5 nm.<sup>12</sup> Different annealing temperatures ranging from 150 to 400 °C have been used to perform the size/gap tuning of the randomly distributed gold nanoisland arrays. Fig. 1 shows the SEM images of the gold nanoisland configurations obtained for different annealing temperatures of (a) 150 °C, (b) 200 °C, (c) 300 °C, and (d) 400 °C (Figures S1, S2 in supporting information show more images of samples annealed at temperatures ranging from 140 °C to 500 °C). It can be observed clearly that both the size and the separation distance (gap width) between the gold nanoislands change with the annealing temperature. The two quantities are not independent, both increase with increasing annealing temperature. From Fig. 1(a) and (b), we find that the distance between the adjacent nanoislands is already too small to be resolved by the SEM imaging. This is caused by the fact that at low annealing temperatures the gold nanoparticles getting molten tend to aggregate to form larger ones, however, the larger ones solidify out since the larger sizes correspond to higher melting point. Since the annealing temperatures of 150 and 200°C are close to the threshold of the melting point of the gold nanoparticles, the size, as well as the gap width, has a relatively large dynamic range. Consequently, the thin layer of gold nanostructures actually consist of a kind of 3D aggregates of gold

nanoparticles with their diameter and separation distance varying in a large dynamic range. Nevertheless, the substrate exhibits excellent homogeneity over its effective area. Thus, low annealing temperatures favor the formation of extremely small gaps between gold nanoparticles and high density of “hot-spot”. In the SEM image of the sample annealed at 200 °C, it can be seen that larger and smaller gold nanoparticles coexist. It can be anticipated that the larger ones may induce more intensive localized field due to plasmonic excitation, so that even stronger SERS enhancement may be achieved.

When the annealing temperature is increased to 300 °C, gold nanoislands with an average diameter of about 70 nm and a typical separation distance larger than 10 nm were produced, as shown in Fig. 1(c). As the annealing temperature is increased to 400 °C, both the size and the shape of the gold nanoislands become more homogeneous and the separation distance between them becomes even larger, as shown in Fig. 1(d). Such large gap widths as found in Fig. 1(c) and (d) reduce significantly the coupling between the adjacent gold nanoislands leading to dramatically reduced electric fields on the “hot-spot” sites.

Since a larger size of the gold islands may induce stronger localized fields due to the stronger plasmonic resonance, an arrangement of larger gold nanoislands with small gap widths is preferred for obtaining a large SERS enhancement. However, in practical situations, smaller gap width and larger gold nanoparticles cannot be achieved simultaneously in one processing step, as demonstrated in Fig. 1. To illustrate this more clearly, enlarged SEM images are presented in Fig. S1 of the supporting information, which show that size and the gap width of the gold nanoislands increase simultaneously with increasing annealing temperature. This is the main feature of the gap/size control approach based on a single processing step,

which is confirmed further by more experimental results in Fig. S2.

Thus, a compromise is required. On the one hand, increasing gap width means weaker hot spots and, on the other hand, the plasmonic excitation of larger nanoislands is stronger. Consequently, there exists an optimized combination of the size and the separation distance of the gold nanoparticles. Both threshold temperatures for the melting of the gold nanoparticles and for the sublimation of the ligands covering the gold nanoparticles are about 150 °C. Fortunately, as will be demonstrated by the experimental results, the optimized annealing temperature is higher than these threshold values.

Further improvement may be achieved in the future using larger colloidal gold nanoparticles with diameters of more than 20 nm. Then, the melting process of the gold nanoparticles can be prevented at higher annealing temperatures. Alternatively, one may attempt to use two subsequent processing steps, the first at a higher annealing temperature where large nanoislands are produced and the second at a lower annealing temperature to produce smaller particles in the gaps of the larger ones. Both approaches are currently under investigation.

To test the SERS substrates, the samples annealed at different temperatures were first immersed in  $10^{-4}$ -M-4-Mercaptopyridine (4-MPy)/ethanol solution for 24 h. After extensive rinsing with ethanol, the samples were finally dried under nitrogen. This procedure leads to the formation of a monolayer of 4-MPy molecules bound to the gold nanoisland structures, which may serve as a probe of the SERS effect.

### **3 Performance of the SERS substrates consisting of gold nanoislands with controllable gap-size landscape**

#### **3.1 Optical spectroscopic performance**

The optical extinction spectra of the SERS substrates in air shown in Fig. 2(a) have been measured using a Shimadzu UV-3600 spectrophotometer. A fairly broad extinction spectrum extending from 520 to 920 nm (at FWHM) can be observed for the sample annealed at 200 °C in contrast to the spectra of the samples annealed at 150, 300, and 400 °C. We attribute this broadening effect to the following mechanisms: (1) relatively wide size distribution of the gold nanoislands.<sup>13</sup> (2) a strong plasmonic coupling between the adjacent nanoislands due to the small gaps between them.<sup>14</sup> When the annealing temperature is increased to 300 °C or 400 °C, the extinction spectra are both peaked around 560-570 nm and their bandwidths become narrower than 100 nm at FWHM. This implies a much more homogeneous distribution of the size and shape of almost isolated gold nanoislands, in concordance with the SEM images in Fig. 1(c) and (d). For the samples annealed at 150 °C, the peak of the extinction spectrum is red-shifted to about 675 nm and has a bandwidth of about 180 nm at FWHM. This indicates some aggregations of smaller gold nanoparticles with true contacts, so that the plasmonic resonance partly results from the bodies of the aggregates, instead of from the isolated small particles. The photographs of the substrates described above are shown in Fig. 2(b) and the change of their colors implies the spectral shift of localized surface plasmon resonance.

### 3.2 SERS enhancement

The SERS spectra of the samples covered with a monolayer of 4-MPy were measured by a Renishaw inVia-Reflex micro-Raman spectrometer equipped with 532 nm, 633 nm, and 785 nm laser sources, and a confocal microscope. A 50× objective (numerical aperture NA = 0.85) was used for all of the measurements. SERS spectra were obtained with incident laser powers of 25 mW at 532 nm, 8.5 mW at 633 nm, and 30 mW at 785 nm, and with an acquisition time of 20 seconds. The SERS substrates

shown in Fig. 1 have been employed in the Raman experiments described below.

SERS spectra for 785-nm excitation are shown in Fig. 3. The maximum SERS enhancement was observed for the substrate annealed at 200°C. The global enhancement factors (EFs) were calculated following the procedures reported in Ref. 15 with the effective area of gold nanoislands and the spot diameter at the focus taken into account. Using the SERS peak at 1001  $\text{cm}^{-1}$  (852 nm) as the reference, the enhancement factor (EF) has been calculated to be as large as  $9.0 \times 10^6$  and  $5.2 \times 10^6$  for the 200-°C- and 150-°C-annealed samples, respectively. However, when the annealing temperature is increased to 300 and 400 °C, no enhancement in the SERS signal can be observed at 785-nm excitation, where only the second order Raman peak of silicon around 930-960  $\text{cm}^{-1}$  can be detected. Thus, no “hotspots” have been produced on these substrates.

When altering the excitation wavelength to 633 nm, the Raman signals from 1001  $\text{cm}^{-1}$  (676 nm) to 1600  $\text{cm}^{-1}$  (705 nm) are all enhanced significantly, as shown in Fig. 4 for the substrates annealed at 150 and 200 °C, which demonstrates stronger plasmonic enhancement for 633 nm excitation as it is closer to the peak plasmon resonance than 785 nm excitation. The enhancement factors at 1001  $\text{cm}^{-1}$  were calculated to be  $9.8 \times 10^6$  and  $5.8 \times 10^6$  for the samples annealed at 200 and 150 °C respectively. However for 633-nm excitation, SERS signals were also observed for the samples annealed at 300 and 400 °C, and the corresponding enhancement factors were calculated to be  $9.1 \times 10^5$  and  $7.0 \times 10^5$ , respectively, which are one order of magnitude lower than those of the samples annealed at 150 and 200 °C. This demonstrates that a better matching of the excitation with the plasmon resonance still leads to considerably enhanced SERS signals even though the large gap-sizes do not

favor the formation of hotspots.

Experimental results by McFarland et al. in Ref. [16] gave more insights into mechanisms how stronger SERS signals were excited by a laser at 633 compared with 785 nm. The relationship between the plasmonic extinction spectrum and the excitation wavelengths has been investigated in Ref. 16. The strongest SERS signal occurred when the excitation laser wavelength was close to and on the higher-energy side of the peak wavelength of plasmon resonance, whereas, the Raman shift was close to and on the lower-energy side of the plasmonic peak. In our results, the extinction peak is around 670 nm for the sample annealed at 150 °C. Thus, the excitation laser at 633 nm is on the higher-energy side and closer to the peak wavelength of 670 nm than 785 nm. However, the extinction spectrum for the sample annealed at 200 °C is broad and the highest peak is at 570 nm. Therefore, the excitation at 633 nm is again closer to the plasmonic extinction peak than 785 nm, although both of the excitation wavelengths are on the lower-energy side of the extinction peak.

A series of experiments using 532-nm excitation have also been performed on the same series of SERS substrates, which are included in Fig. S3 of the supporting information. In this case, only very weak Raman signals have been detected, implying that 532 nm as excitation wavelength is not a good choice, although this wavelength is within the spectral band for effective plasmon excitation (Fig. 2). This can be understood by considering that the enhancement factor increases with the absolute value of the ratio between the real and the imaginary part of the permittivity of metals defined as  $|\epsilon'/\epsilon''|$ .<sup>17,18</sup> For gold, this ratio increases with the increase in the excitation wavelength in the spectral range from 500 to 900 nm, where the ratio increases from  $\sim 1$  to 33.<sup>19</sup>

The enhancement factor is also affected by the size of the metallic nanostructures.<sup>20</sup> In principle, larger gold nanoparticles induce stronger localized fields than smaller ones. However, the gap between them plays a more important role in the creation of hotspots with extremely intensive local field. Therefore, there exists a compromise between the two parameters for optimization. In fact, it is very difficult to achieve extremely small gaps while keeping large sizes of the gold nanostructures currently. On the other hand, too small sizes of the gold nanoparticles may result in the aggregation with true contacts of the smaller particles, which actually destroys the plasmonic response of the gold nanoparticles. Above mechanisms determined the final optimized configuration of the SERS substrates and explain why the best SERS performance has been obtained by the substrate annealed at 200 °C, as compared with those annealed at 150, 300, and 400 °C.

### 3.3 Large-area homogeneity

To characterize the homogeneity of SERS enhancement over the whole substrate area, the main vibration of 4-MPy has been measured in “mapping” mode by a WITec Alpha300A confocal Raman spectrometer equipped with a synapse CCD detector and a 633 nm He–Ne laser. A 100× objective (numerical aperture NA = 0.9) was used in all the measurements, and the light spot at the focus is about 858 nm in diameter. More than 62500 spectra were collected in the “mapping” image shown in Fig. 5(a). The intensity of the Raman vibrational signal at 1001 cm<sup>-1</sup> on an area of 50×50 μm<sup>2</sup> is plotted in Fig. 5(a), and the average SERS spectra on bright and dark spots are shown in Fig. 5(b) and (c), respectively, which are marked by dotted circles in Fig. 5(a). The average spectrum all over the mapping area was shown in Fig. 5(d). It is demonstrated convincingly in Fig. 5 that the main Raman vibrations of 4-MPy for the aromatic ring breathing modes (1001, 1017, 1060, and 1097 cm<sup>-1</sup>) were enhanced at

all spots with high contrast and clear boundary, indicating excellent SERS activity. The difference between the amplitude of the SERS signals on the dark and bright spots was  $\sim 20$  CCD counts. The relative standard deviation (RSD) of the Raman intensity was calculated with more than 200 spectra, which was 5.1% and 5.4% for Raman vibrations at 1001 and 1017  $\text{cm}^{-1}$ , respectively, for the 200 °C annealed samples. These results are much better than the data reported previously<sup>7,8</sup> and show highly homogeneous SERS activity over the whole substrate area.

### 3.4 Near-field investigation

Electromagnetic near-field distributions around the randomly distributed gold nanoislands in different assemblies were calculated using the finite-difference time-domain (FDTD) method,<sup>20</sup> as shown in Fig. 6. Typical parameters for theoretical calculations have been chosen on the basis of the statistic results of Fig 1 with the help of the image-Pro® Plus software (from Media Cybernetics Inc.). The mean-diameter distribution of the gold nanoislands corresponding to the configuration with strongest SERS enhancement in Fig. 1(b) was calculated and the results are shown in Fig. S4 in the supporting information. We found that the mean diameter of the annealed gold nanoislands has two distribution regions, one is peaked at about 20 nm and the other at about 50 nm. Different combinations between two kinds of gold nanoparticles with diameters of 20 and 50 nm and different gap widths of 1, 4, and 16 nm are investigated. The sizes of the gold nanoparticles have been chosen on the basis of the analysis (as shown in Fig. S4) of the SEM image in Fig. 1(b), corresponding to the configuration with strongest SERS activity. The intensity of the electric field on the “hotspots”, which are found located exactly at the gap, is strongly dependent on the distance between the gold nanoparticles or the gap width. A smaller gap induces much stronger electric fields (Fig. 6(a), (d), (g)). Furthermore, larger gold

nanoparticles excite a much larger volume of electric field with higher strength (Fig. 6(a)). Fig. 7 shows the variation of the intensity of electric field with the gap width for three combinations between the two kinds of gold nanoparticles and for the two excitation wavelengths of 633 and 785 nm. The intensity of the electric field decreases nearly exponentially with increasing gap width between the gold nanoparticles. For the same gap width ( $d$ ), the electric field is much stronger for the gold nanoparticles with a larger diameter ( $D = 50$  nm) than for those with a smaller diameter ( $D = 20$  nm). However, the intensity of the electric field is reduced dramatically as the two gold nanoparticles get into contact ( $d = 0$ ). Moreover, 633-nm excitation induces much stronger fields than 785-nm in agreement with the experimental findings. The reason is that 633 nm is much closer to the position in the extinction spectra that the incident and Raman scattered photons are both strongly enhanced.<sup>16</sup>

In order to compare the samples annealed at 200 and 300 °C, further simulations were performed on the basis based on Fig. 1(c) and Fig. S1(d). The simulation results are given in Fig. S5 of the supporting information. Three gap widths of 3, 10, and 30 nm and two diameters of 40 and 70 nm have been used for the gold nano-island matrix in the simulations. Although very strong local field can be observed for gap widths of 3 and 10 nm in Fig. S5, the practical gap width was measured to be larger than 10 nm in Fig. 1(c), leading to much reduced local field.

A numerical comparison of the local-field intensity following the simulation results in Fig. S5 was given by Fig. S6. When we compare the red curve in Fig. 7 and the black curve in Fig. S6, which correspond closely to samples annealed at 200 and 300 °C, respectively, we can find that the former is more than an order stronger than the later in intensity. This explains convincingly why SERS signal became weaker when the

temperature is increased to higher than 200 °C.

#### 4 Conclusions

In conclusion, we demonstrate a cheap and highly reproducible approach for fabricating SERS substrates with excellent homogeneity over an effective area of  $2 \times 2 \text{ cm}^2$  and global SERS enhancement factors in the order of  $10^7$  for 633-nm excitation. The SERS spectroscopic measurements show that fluctuations of the global SERS enhancement over the sample area are less than 5.4% by RSD. There exist optimized configurations of the size and gap width of the gold nanostructures that have been patterned randomly on glass or silicon substrates through annealing spin-coated colloidal gold nanoparticles. The corresponding broadband plasmonic resonance covering the excitation wavelengths at 633 and 785 nm ensured strong SERS activities.

#### 5 Acknowledgements

We acknowledge the 973 program (2013CB922404), the National Natural Science Foundation of China (11304005, 11274031, 11104007), and Beijing Natural Science Foundation (4133082, 1132004), the Beijing Educational Commission (KM201210005034) and the Specialized Research Fund for the Doctoral Program of Higher Education (20121103120001).

## Reference

1. S. Nie, and S. R. Emory, Probing Single Molecules and Single Nanoparticles by Surface-Enhanced Raman Scattering, *Science* **275**, 1102 (1997).
2. S. Y. Lee, E. Ganbold, J. S. Choo, and W. Joo, Detection of Melamine in Powdered Milk Using Surface-Enhanced Raman Scattering with No Pretreatment, *Anal. Lett.* **43**, 2135 (2010).
3. S. Q. Liu, and Z. Y. Tang, Nanoparticle assemblies for biological and chemical sensing, *J. Mater. Chem.* **20**, 24 (2010).
4. Q. M. Yu, P. Guan, D. Qin, G. Golden, and P. M. Wallace, Inverted Size-Dependence of Surface-Enhanced Raman Scattering on Gold Nanohole and Nanodisk Arrays, *Nano Lett.* **8**, 1923 (2008).
5. C. L. Haynes, and R. P. Van Duyne, Nanosphere Lithography: A Versatile Nanofabrication Tool for Studies of Size-Dependent Nanoparticle Optics, *J. Phys. Chem. B* **105**, 5599 (2001).
6. A. Lesuffleur, L. K. Kumar, A.G. Brolo, K. L. Kavanagh, and R. Gordon, Apex-Enhanced Raman Spectroscopy Using Double-Hole Arrays in a Gold Film, *J. Phys. Chem. C* **111**, 2347 (2007).
7. W. Lee, S. Y. Lee, R.M. Briber, and O. Rabin, Self-Assembled SERS Substrates with Tunable Surface Plasmon Resonances, *Adv. Funct. Mater.* **21**, 3424 (2011).
8. R. H. Que, M. W. Shao, S. J. Zhuo, C. Y. Wen, S. D. Wang, and S. T. Lee, Highly Reproducible Surface-Enhanced Raman Scattering on a Capillarity-Assisted Gold Nanoparticle Assembly, *Adv. Funct. Mater.* **21**, 3337 (2011).
9. Y. Q. Wen, W. Q. Wang, Z. L. Zhang, L. P. Xu, H. W. Du, X. J. Zhang, and Y. L. Song, Controllable and reproducible construction of a SERS substrate and its sensing applications, *Nanoscale* **5**, 523 (2013).
10. U. S. Dinish, F. C. Yaw, A. Agarwal, and M. Olivo, Development of highly reproducible nanogap SERS substrates: Comparative performance analysis and its application for glucose sensing, *Biosens. Bioelectron.* **26**, 1987 (2011).
11. M. J. Hostetler, J. E. Wingate, C. J. Zhong, J. E. Harris, R. W. Vachet, M. R. Clark, J. D. Londono, S. J. Green, J. J. Stokes, G. D. Wignall, G. L. Glish, M. D. Porter, N. D. Evans, and R. W. Murray, Gold Cluster Molecules with Core Diameters from 1.5 to 5.2 nm: Core and

- Monolayer Properties as a Function of Core Size, *Langmuir* **14**, 17 (1998).
12. P. Buffat, and J. P. Borel, Size effect on the melting temperature of gold particles, *Phys. Rev. A* **13**, 2287 (1976).
  13. J. C. Martínez, N. A. J Chequer, L. González, and T. Cordova, Alternative Methodology for Gold Nanoparticles Diameter Characterization Using PCA Technique and UV-VIS Spectrophotometry, *Nanosci. Nanotechnol.* **2**, 184 (2012).
  14. J. Kumar, X. Z. Wei, S. Barrow, A. M. Funston, K. G. Thomas, and P. Mulvaney, Surface plasmon coupling in end-to-end linked gold nanorod dimers and trimers, *Phys. Chem. Chem. Phys.* **15**, 4258 (2013).
  15. E. C. Ru, E. Blackie, M. Meyer, and P. G. Etchegoin, Surface Enhanced Raman Scattering Enhancement Factors: A Comprehensive Study, *J. Phys. Chem. C* **111**, 13794 (2007).
  16. A. D. McFarland, M. A. Young, J. A. Dieringer, and R. P. Van Duyne, Wavelength-Scanned Surface-Enhanced Raman Excitation Spectroscopy, *J. Phys. Chem. B*, **109**, 11279 (2005).
  17. U. Kreibig, and M. Vollmer, *Optical Properties of Metal Clusters*, Springer, Berlin, 1995.
  18. I. D. Mayergoyz, Z. Zhang, and G. Miano, Analysis of Dynamics of Excitation and Dephasing of Plasmon Resonance Modes in Nanoparticles, *Phys. Rev. Lett.* **98**, 147401 (2007).
  19. E. Palik, and G. Ghosh, *Handbook of Optical Constants of Solids*, Academic Press, Boston 1998.
  20. R. Thomas, and R. S. Swathi, Organization of Metal Nanoparticles for Surface-Enhanced Spectroscopy: A Difference in Size Matters, *J. Phys. Chem. C* **116**, 21982 (2012).

## Figure Captions

Fig. 1 SEM images of gold nano-island structures obtained at different annealing temperatures: (a) 150°C, (b) 200°C, (c) 300°C, and (d) 400°C. Insets in (a) and (b) are the enlarged SEM images of the structures annealed at 150 and 200°C.

Fig. 2 (a) Normalized optical extinction spectra of the SERS substrates obtained at different annealing temperatures of 150°C, 200°C, 300°C, and 400°C in air. The vertical dashed lines indicate the wavelengths of the incident light utilized in our SERS measurements; (b) Photograph of SERS structures prepared on glass substrate. From left to right, the samples with different colors correspond to the substrates annealed at 150°C, 200°C, 300°C and 400°C, respectively.

Fig. 3 SERS spectra with 785-nm excitation of the 4-MPy modified gold nano-island structures annealed at different temperature.

Fig. 4 SERS spectra with 633-nm excitation of the 4-MPy modified gold nano-island structures annealed at different temperature.

Fig. 5 (Left panel) (a) The “mapping” image on an area of  $50 \times 50 \mu\text{m}^2$  for the Raman vibration at  $1001 \text{ cm}^{-1}$  of a 4-MPy monolayer on SERS sample annealed at 200 °C annealed. (Right panel) The average SERS spectra on bright (b) and dark (c) spots which are marked by dotted circles in image (a), and the average SERS spectrum all over the mapping area (d).

Fig. 6 Electric field intensity distribution profiles in the vicinity of the Au nanoparticle dimers as a function of the gap size for “ || ” polarization of the incident light with

633-nm excitation. Scale bar: 20 nm; The diameters ( $D$ ) of the Au nanoparticle dimers are 50-50nm, 50-20nm and 20-20nm; three typical gap width as  $d=1$ nm, 4 nm and 16 nm have been calculated; the red arrows in the images are the direction of the incident polarization.

Fig. 7 Variation of the intensity of electric field with the gap width for three combinations between the two kinds of gold nanoparticles ( $D=20$  nm and 50 nm) and for two excitation wavelengths at 633 and 785 nm with “ $\parallel$ ” polarization.

## Figures

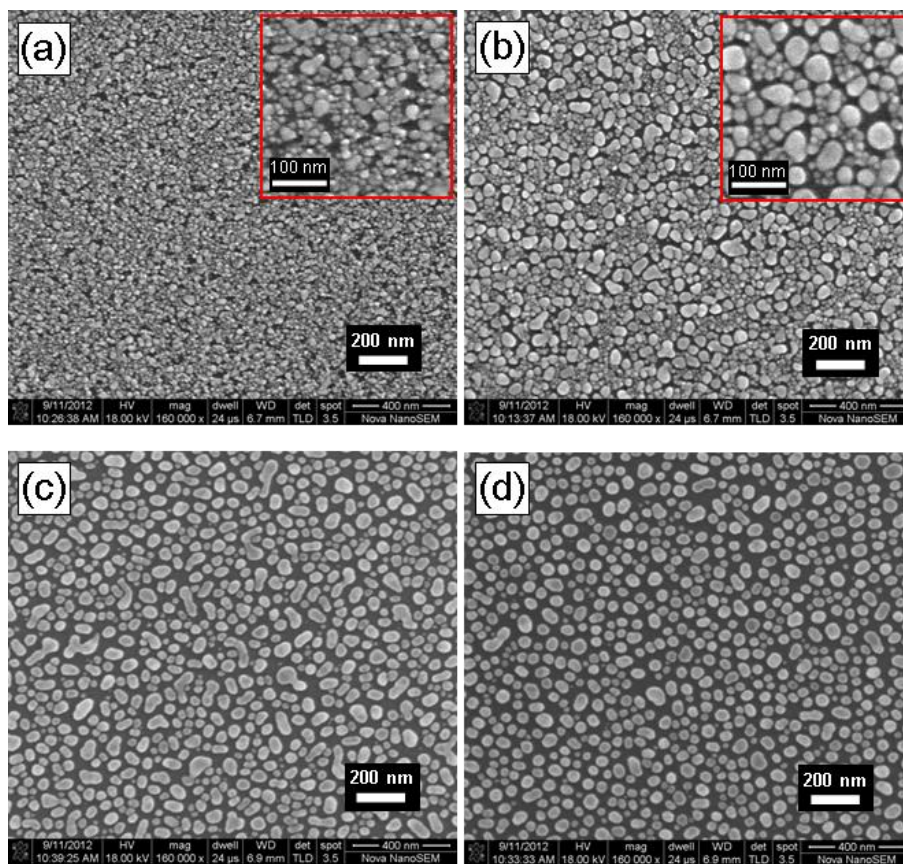


Fig. 1

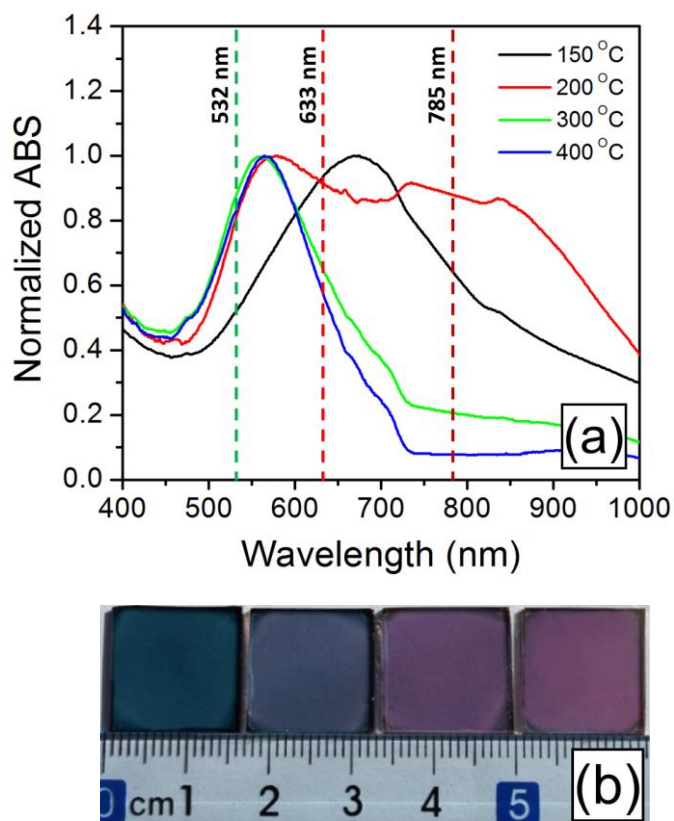


Fig. 2

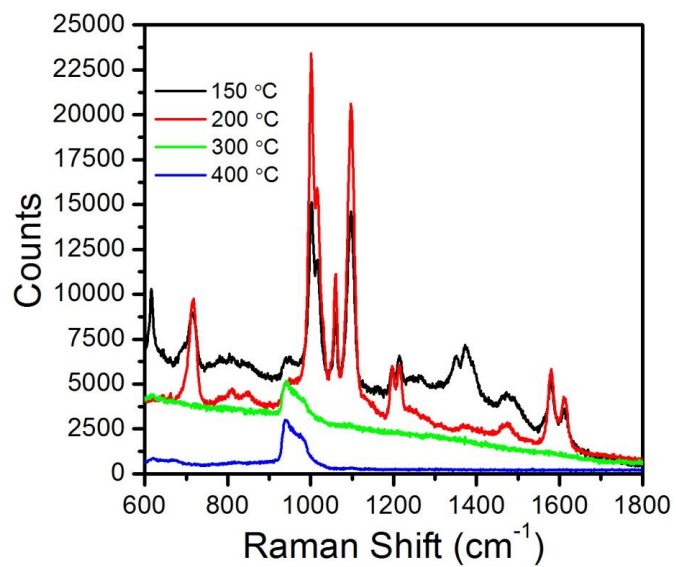


Fig. 3

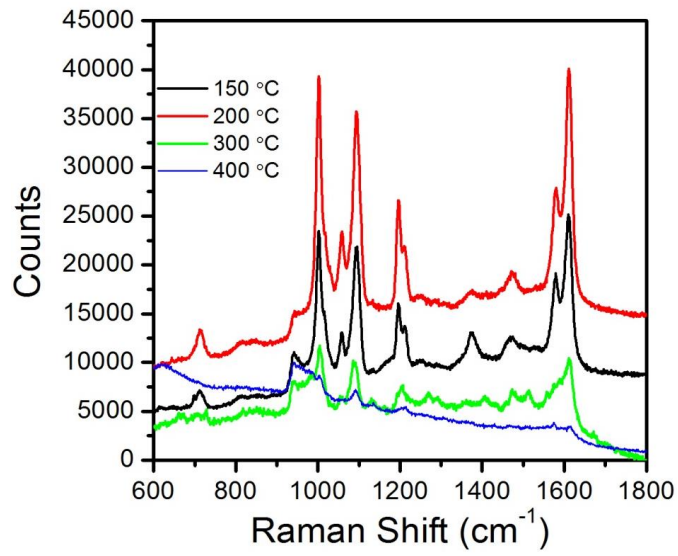


Fig. 4

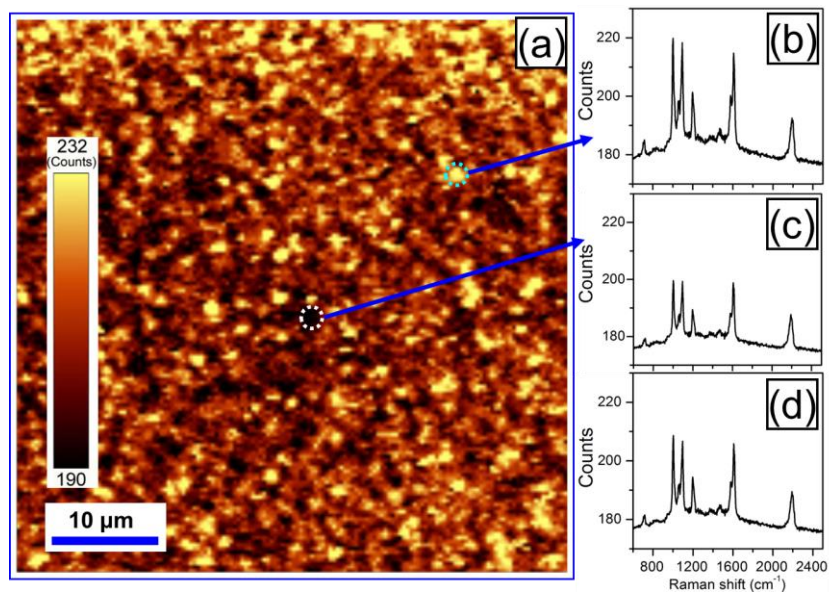


Fig. 5

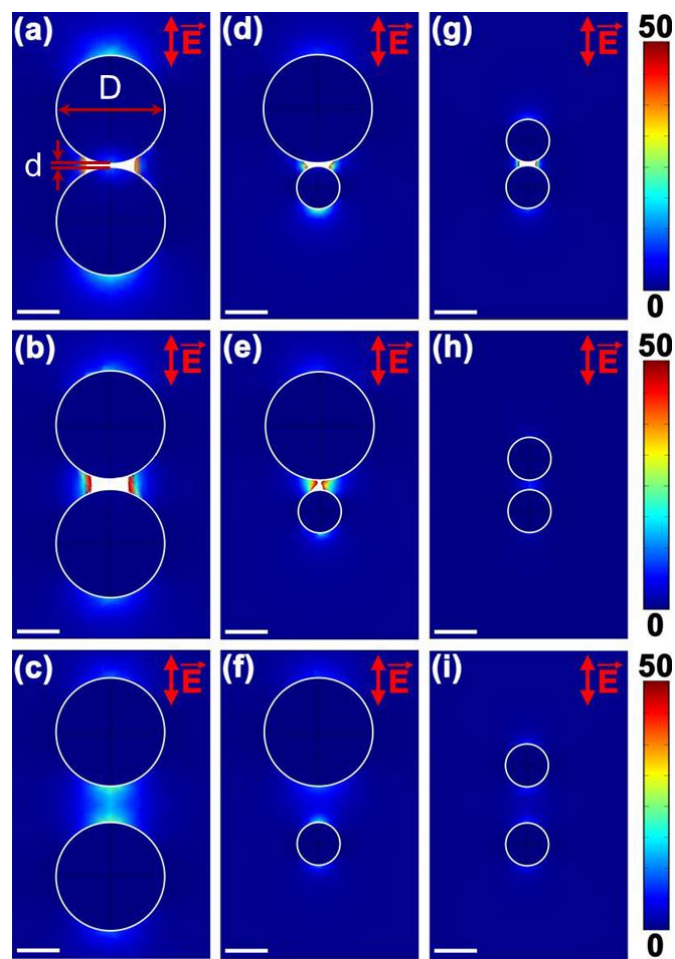


Fig. 6

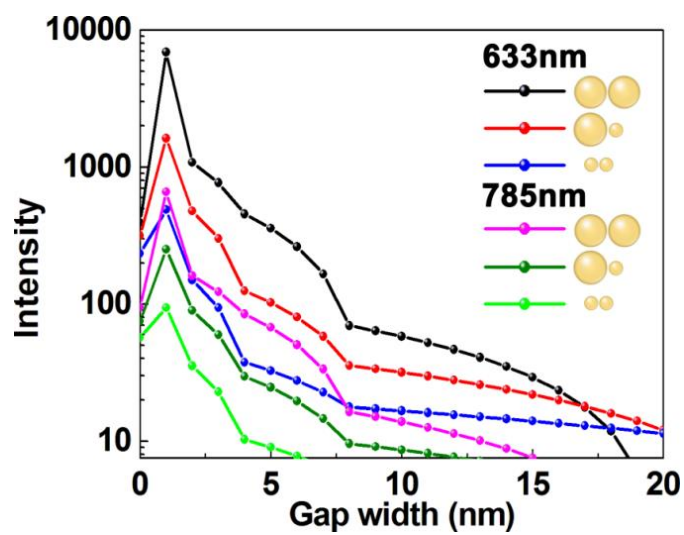


Fig. 7